Outer-layer similarity in the presence of a practical rough-wall topography

Y. Wu and K. T. Christensen[a)]
Department of Mechanical Science and Engineering, University of Illinois at Urbana-Champaign, Urbana, Illinois 61801, USA

(Received 24 February 2007; accepted 25 April 2007; published online 24 August 2007)

High-resolution particle image velocimetry measurements are made in the streamwise–wall-normal plane of a zero-pressure-gradient turbulent boundary layer over smooth and rough walls at $\mathrm{Re}_\theta \approx 13000$. The roughness considered herein is replicated from a surface scan of a turbine blade damaged by deposition of foreign materials and its topography is highly irregular and contains a broad range of topographical scales. Two physical scalings of the same roughness topography are considered, yielding two different rough surfaces: RF1 with $k=4.2$ mm and RF2 with $k=2.1$ mm, where k is the average peak-to-valley roughness height. At $\mathrm{Re}_\theta \approx 13000$, these roughness conditions yield $k^+ \equiv k/y_* = 207$, $\delta/k = 28$, $k_s^+ = 115$, and $\delta/k_s = 48$ for RF1 and $k^+ = 91$, $\delta/k = 50$, $k_s^+ = 29$, and $\delta/k_s = 162$ for RF2 (where δ is the boundary-layer thickness, k_s is the equivalent sand-grain height, and y_* is the viscous length scale). The mean velocity deficits along with the Reynolds normal and shear stress profiles for both roughness conditions collapse on the smooth-wall baseline in the outer layer when appropriately scaled by the friction velocity, u_τ. Probability density functions and quadrant analysis of the instantaneous events contributing to the mean Reynolds shear stress show similar outer-layer consistency between the smooth and rough cases when scaled appropriately with u_τ. In addition, one-dimensional, two-point streamwise, and wall-normal velocity autocorrelation coefficients are also found to collapse in the outer region, indicating a similarity in the spatial structure of the outer-layer turbulence. The observed collapse of the smooth- and rough-wall turbulence statistics in the outer layer supports Townsend's wall similarity hypothesis for flow over the unique surface topography considered herein. © *2007 American Institute of Physics*.
[DOI: 10.1063/1.2741256]

I. INTRODUCTION

Most practical wall-bounded turbulent flows of interest, such as flows over turbine blades, through heat exchangers, and over aircraft and ship hulls, are influenced by surface-roughness effects. In some applications, surface defects are small on an absolute scale yet can still be hydrodynamically important if they are large relative to the viscous length scale of the turbulence [i.e., at high Reynolds number (Re)]. In addition, the surface conditions in practical wall-bounded flows can often degrade over time, from hydraulically smooth prior to deployment to significantly roughened over time due to harsh operating conditions. Examples of such conditions include cumulative damage to turbine blades,[1] cumulative algae/barnacle buildup on the surfaces of submarines and ships,[2] and surface erosion observed on the blades of windmills operating near the sea. In most cases, surface roughness significantly increases the wall shear stress and can augment heat and mass transfer at the wall, resulting in an increase in the thermal loading of a system. This latter effect can severely reduce the lifetime of vital parts of many practical engineering systems (such as turbine blades). Therefore, a clear understanding of the impact of surface roughness on wall turbulence is imperative for successful modeling and control of these flows. Such advances will likely lead to profound improvements in the overall efficiency and lifetime of a multitude of practical engineering systems.

Rough-wall turbulence has received intense research attention for the last several decades, and the review articles by Raupach *et al.*[3] and Jimenez,[4] for example, provide thorough summaries of the knowledge gleaned from this research. It is generally accepted that within the roughness sublayer, $\sim 3-5k$ away from the wall (where k is a measure of the roughness height), the turbulence is strongly affected by the surface conditions. However, conflicting evidence exists as to whether roughness effects penetrate *beyond* the roughness sublayer and into the outer layer of the flow. Townsend[5] first hypothesized that at high Reynolds numbers, the turbulent motions in the outer layer are independent of surface conditions and viscosity except for their role in setting the wall shear stress (and hence the friction velocity, $u_\tau = [\tau_w/\rho]^{1/2}$) and the boundary-layer thickness, δ. With respect to rough-wall flows, this hypothesis implies that if the characteristic height of the roughness, k, is sufficiently small compared to δ, then the direct impact of roughness is confined within the viscous dominated roughness sublayer. Under such conditions, the turbulence in the outer layer is only indirectly influenced by roughness through its role in determining u_τ and δ.[3] Since this wall similarity hypothesis was first proposed, many studies have indeed observed the various statistics of smooth- and rough-wall flows, including the mean velocity deficit as well as profiles of the Reynolds normal and shear stresses, to behave similarly outside the roughness sublayer

[a)]Electronic mail: ktc@uiuc.edu

TABLE I. Past studies that observe wall similarity. BL, boundary layer; TC, turbulent channel; TP, turbulent pipe.

Studies	Flow	Roughness	k^+	k_s^+	δ/k	δ/k_s
Raupach (1981)[6]	BL	Cylinders	337–427	–	19–129	–
Ligrani and Moffat (1986)[9]	BL	Spheres	22–63	–	–	–
Bandyopadhyay and Watson (1988)[10]	BL	2D grooves	15–18	–	60	–
Flack *et al.* (2005)[7]	BL	Sandpaper	134	100	46.2	62.5
		Woven mesh	64	138	97.2	45.5
Schultz and Flack (2003)[39]	BL	Sandpaper	7.6–32	7–126	32.5–120	175–232
Schultz and Flack (2005)[27]	BL	Spheres	35–182	–	30–34	–
Grass (1971)[40]	BL	Sand	21	21	24	24
		Pebbles	85	–	6.5	–
Krogstad *et al.* (2005)[41]	TC	2D grooves	13.6–20.4	63–121	30	5–6
Bakken *et al.* (2005)[42]	TC	2D grooves	20–200	60–1560	30	6–10
		Woven mesh	15–187	30–617	33	9–15
Allen *et al.* (2007)[20]	TP	Honed surface	0.06–14.8	0.17–44.4	51500	17000

when appropriately scaled by u_τ. In particular, wall similarity has been observed for turbulent flow over a variety of roughness topographies, including cylindrical roughness,[6] sand-grain,[7] mesh,[7,8] spheres,[9] and two-dimensional grooves.[10] However, it should be noted that all of these topographies are *idealized* in the sense that they are characterized by a dominant topographical scale arranged in an ordered manner. Further, these studies span a broad range in both Re, inner-scaled roughness height ($k^+ \equiv k/y_*$) and scale separation (δ/k), although it is generally accepted that the roughness sublayer and the outer region of the flow must be sufficiently separated for wall similarity to exist, implying $\delta \gg k$. However, despite the fact that k is a physically meaningful measure of the characteristic roughness height, rough-wall flows are generally classified as hydraulically smooth ($k_s^+ < 5$), transitionally rough ($5 < k_s^+ \lesssim 70$), and fully rough ($k_s^+ \gtrsim 70$) via an equivalent sand-grain height, k_s, which relates arbitrary roughness topographies to the sand-grain experiments of Nikuradse[11] through the roughness function, ΔU^+. As such, k_s is not a representative topographical scale for a given roughness topography (unless the roughness is sand grain) but simply relates the bulk impact of an arbitrary roughness on the mean flow to sand grain of height k_s. Table I summarizes the salient details of many of the aforementioned studies that observe wall similarity. Interestingly, the common feature between these studies is actually not a threshold on k^+ or k_s^+ as similarity is observed for both transitionally and fully rough flows. Instead, the common thread among these efforts is a substantial separation between the roughness scale and the outer length scale of the flow via large δ/k or δ/k_s. It should be noted that Jimenez[4] proposed a criterion for the existence of wall similarity based on the physical roughness height k ($\delta/k \gtrsim 40$) while Flack *et al.*[7] recently proposed a threshold based on k_s ($\delta/k_s \gtrsim 40$).

Despite significant evidence supporting the validity of Townsend's wall similarity hypothesis in the presence of many different idealized roughness topographies, other studies have indicated substantial modification of the outer layer in the presence of roughness. In particular, Krogstad[12] observed strong outer-layer effects imposed by woven mesh, including modifications of the mean velocity profile and the Reynolds stresses. Numerous other recent studies over different idealized rough surfaces[13–15] also indicate that wall similarity may not be a universal characteristic of rough-wall turbulence. The pertinent details of these studies are summarized in Table II, and the most obvious common feature among them appears to be rather weak separation between the roughness and outer length scales. In particular, while a number of these studies have relatively large δ/k values, nearly all of them have relatively small values of δ/k_s.

TABLE II. Past studies that do not observe wall similarity. BL, boundary layer; TC, turbulent channel.

Studies	Flow	Roughness type	k^+	k_s^+	δ/k	δ/k_s
Keirsbulck *et al.* (2002)[15]	BL	2D grooves	150	552	26.3	7.5
Krogstad and Antonia (1999)[14]	BL	Woven mesh	143	352	48	15
		2D grooves	143	287	47	8
Krogstad *et al.* (1992)[12]	BL	Woven mesh	143	352	48	15
Shafi and Antonia (1997)[13]	BL	Woven mesh	54	–	58.4	–
Tachie *et al.* (2003)[43]	BL	Sand	33	33	31	31
		Mesh	17	–	63	–
Tachie *et al.* (2000)[44]	BL	Sand	25–35	25–35	21–29	21–29
		Mesh	17–25	–	67–75	–
Bhaganagar *et al.* (2004)[45]	TC	Egg carton	5.4–21.6	10–48	18.5–74	8–40

Therefore, considering this trend, in concert with the trend noted in the studies supporting outer-layer similarity, it appears that substantial separation between the roughness sublayer and the outer flow in the form of large δ/k_s represents the appropriate condition for the existence of wall similarity. Interestingly, δ/k does not appear to play as strong a role in this regard even though k is more representative of the actual wall-normal extent of the specific topography under consideration.

While the many studies cited above consider the validity of wall similarity in the presence of sand-grain, k- or d-type transverse bars, wire mesh, and ordered arrays of elements, these topographies should be considered highly idealized since they typically contain a single roughness scale arranged in an ordered manner. Unfortunately, the roughness encountered in a variety of technologically relevant applications, such as the surfaces of damaged turbine blades and the surfaces of ships and submarines, can be highly irregular and contain a broad range of topographical scales. In the case of turbine blades, surface roughness is attributable to multiple damage mechanisms, including pitting/erosion, spallation, and/or deposition of foreign materials.[16] Given the complex nature of these practical roughness topographies, it is not clear whether studies of idealized roughness are sufficient for accurately characterizing the turbulent physics in the presence of more practical roughness topographies.

Differences between real and idealized roughness have been known for several decades, most notably discrepancies in friction factor in the transitionally rough regime between Nikuradse's results for sand-grain roughness[11] and Colebrook's relationship based on "industrial" roughness.[17] Acharya *et al.*[18] studied the influence of several different rough surfaces on a turbulent boundary layer, including two stochastically rough surfaces representative of newly finished turbomachinery bladings, namely a sand-cast surface and a mesh surface. Their measurements of velocity defect profiles and Reynolds stresses along the streamwise direction over each rough surface revealed good agreement, although cross comparison between the different surfaces was not provided. Bons *et al.*[16] studied the surface characteristics of a number of in-service land-based turbine blades and vanes. It was observed that different damage mechanisms generate very distinct roughness signatures. Bons *et al.*[16] therefore concluded that it is not likely that a simplified roughness topography, such as an ordered arrays of cones, spheres, or cylinders, will effectively represent the wide range of topographical scales observed in real roughness. In a follow-up study, Bons[1] used scaled replicas of turbine-blade roughness in a turbulent boundary layer to investigate the effects of highly irregular roughness on heat transfer and skin friction coefficients. These efforts revealed that traditional correlations for heat transfer and skin friction severely underestimate the influence of real roughness, particularly in the transitionally rough regime. Further, Subramanian *et al.*[19] extended the work of Bons[1] by considering the single-point turbulence statistics over a short strip of turbine-blade roughness in a turbulent boundary layer. The authors proposed a pressure-gradient velocity scale to account for the pressure variations induced by roughness in this spatially developing flow. Finally, Allen *et al.*[20] studied turbulent pipe flow in the presence of a honed surface akin to the "industrial"-type roughness used by Colebrook[17] in the formulation of the widely used Moody chart. However, their friction-factor results displayed strong deviation from the Colebrook relationship and instead mimicked the friction-factor trends of Nikuradse's sand-grain experiments. Allen *et al.*[20] also presented smooth- and rough-wall mean velocity defect profiles, streamwise turbulence intensity profiles, and streamwise velocity spectra that collapsed in the outer layer in accordance with Townsend's wall similarity hypothesis. These outer-layer similarity observations represent the first of their kind for a more practical surface topography but for extremely large separation between the roughness and outer length scales ($\delta/k \sim 51000$, $\delta/k_s \sim 17000$).

A crucial and lingering question in rough-wall turbulence is whether wall similarity can be expected in the presence of nonideal surface topographies that are highly irregular at more moderate δ/k and/or δ/k_s (i.e., closer to the thresholds proposed by Jimenez[4] and Flack *et al.*[7]). Such behavior is characteristic of many practical flow systems wherein the surface conditions degrade significantly over time. If such similarity is observed in the presence of such surfaces, then outer-layer modeling of many practical rough-wall flows could be greatly simplified. To this end, the present effort assesses the validity of Townsend's wall similarity hypothesis in the presence of a practical surface topography. The roughness studied herein is replicated from a surface scan of a turbine blade damaged by deposition of foreign materials and contains a broad range of topographical scales.

II. EXPERIMENTS

Particle image velocimetry (PIV) is used to study the impact of surface roughness replicated from a turbine blade damaged by deposition of foreign materials on a zero-pressure-gradient turbulent boundary layer at $\mathrm{Re}_\theta \equiv U_e\theta/\nu \approx 13000$, where U_e is the free-stream velocity, θ is the momentum thickness, and ν is the kinematic viscosity of the fluid. All measurements are made in an Eiffel-type, open circuit, boundary-layer wind tunnel with a documented turbulence intensity of 0.16% in the free stream.[21] The working section of the tunnel consists of two 3-m-long by 1-m-wide flat plates suspended above the bottom wall of the tunnel that are smoothly joined at the streamwise center. The two rough-wall conditions considered herein are derived from one of the surfaces characterized by Bons *et al.*[16] and subsequently used by Bons[1] to study bulk skin friction and heat transfer characteristics over turbine-blade roughness (a digitized version of surface 4 from Ref. 1 was generously loaned to our group by Professor J. Bons of Brigham Young University). It should be noted that the original profilometry measurements of this damaged turbine-blade surface by Bons *et al.*[16] yielded roughness heights on the order of tens to hundreds of micrometers. Therefore, in order to generate both transitionally and fully rough conditions for the relatively thick boundary layers generated by the flow facility employed ($\delta \sim 100$ mm) at the Re_θ considered herein, the original pro-

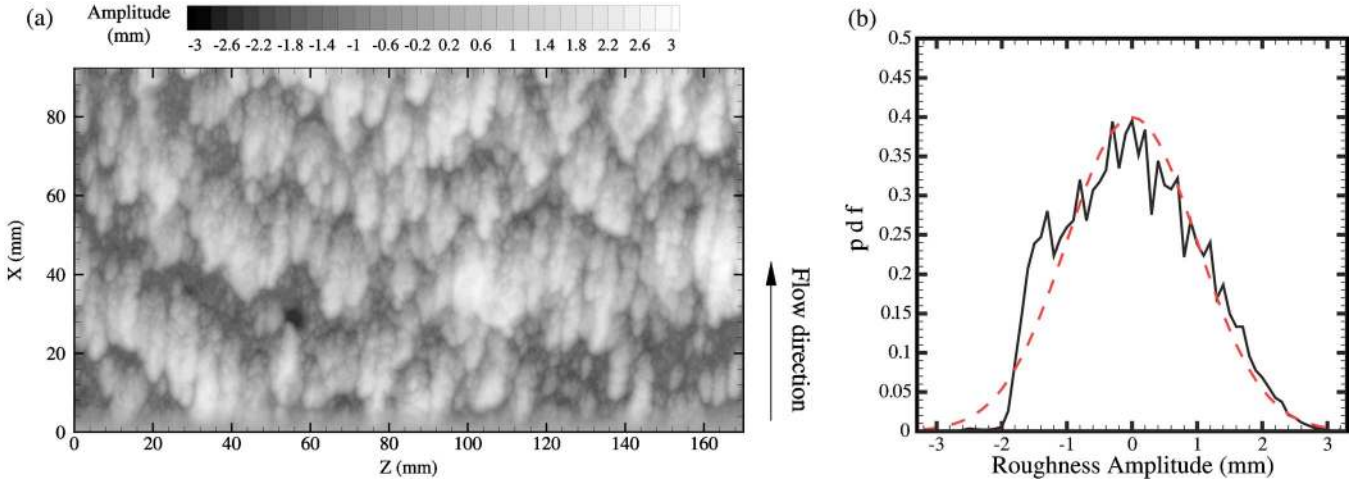

FIG. 1. (a) Contour plot of a portion of the surface topography for the RF1 case. (b) Probability density function (pdf) of the roughness amplitude about the mean elevation for the RF1 case (——) contrasted with a Gaussian distribution with an equivalent rms (– – –).

filometry information was scaled up in all three dimensions to yield two different topographical conditions: one rough-wall condition with $k=4.2$ mm (hereafter referred to as the RF1 case) and an additional rough surface with $k=2.1$ mm denoted the RF2 case. (Following Bons,[1] the characteristic roughness height, k, is taken to be the average peak-to-valley roughness height of the surface.) The root-mean-square (rms) roughness heights, k_{rms}, for the RF1 and RF2 surfaces are 1.0 and 0.50 mm, respectively, while the skewness and flatness of both topographies are 0.19 and 2.35, respectively. Therefore, while the underlying topographical features of RF1 and RF2 are identical in character, the RF2 case is scaled down in all three dimensions by a factor of 2 relative to the RF1 case. Given that the boundary layers under consideration have thicknesses of approximately 100 mm, the RF1 condition gives $\delta/k \approx 25$ while the RF2 condition gives $\delta/k \approx 50$, below and above the threshold of $\delta/k=40$ proposed by Jimenez[4] for the validity of the wall similarity hypothesis (the boundary-layer thickness, δ, is taken as the wall-normal position where the mean streamwise velocity equals 99% of the free-stream velocity for all cases). Separate measurements are made for flow over a smooth wall as well as for flow over each rough-wall condition at similar Re_θ, with the smooth-wall data serving as a baseline against which the roughness data are compared.

Figure 1(a) presents a contour plot of the RF1 scaling. The dominant topographical features of this surface, attributable to deposition of foreign materials, are elliptical in shape and are generally aligned in the streamwise direction. However, a broad range of topographical scales is also clearly evident in this surface. Figure 1(b) presents the probability density function (pdf) of the roughness amplitude about the mean elevation for the RF1 case contrasted with a Gaussian distribution with an equivalent rms. This pdf highlights the broad range of topographical fluctuations that exist about the mean elevation, but, as the aforementioned flatness value of 2.35 suggests, the pdf of the roughness amplitude is not strictly Gaussian. To facilitate testing, the scaled digitized topographies for each roughness case were fed to a three-dimensional powder-deposition printer with 80 μm resolution. This printer constructed replicas of the topography layer-by-layer with a maximum spatial footprint of 25 $\times 30$ cm^2 and a mean thickness of approximately 6 mm. It should be noted that in order to achieve a self-similar rough-wall boundary layer, one must have a sufficient streamwise fetch of roughness ($\sim 15-20\delta$) prior to the measurement location.[22] To achieve such a state, the downstream 3 m (equivalently $\sim 30\delta$) of the flat plate in the wind tunnel was covered with roughness. In order to accommodate these roughness panels, the upstream half of the flat plate was raised relative to the downstream half such that the mean elevation of the roughness was coincident with the upstream smooth wall. Further, since the original spatial footprint of the digitized topography is certainly not sufficient to fill this large an area, the topography was mirrored in both the streamwise and spanwise directions to achieve an appropriate streamwise fetch of roughness. This mirroring required the reproduction of over 80 individual roughness panels for each case (RF1 and RF2). These panels were mounted to cast aluminum plates that were then laid along the downstream half of the wind tunnel. The flow is tripped with a cylindrical rod prior to the leading edge of the roughness, and all measurements are made 2.5 m ($\sim 25\delta$) downstream of its leading edge.

Over 2500 statistically independent, two-dimensional velocity (u,v) fields are acquired by PIV in the streamwise–wall-normal (x,y) plane for each surface condition (smooth, RF1 and RF2) to minimize sampling errors in the computed statistics. Figure 2 presents a schematic of the experimental setup. The flow field is illuminated with a 500-μm-thick laser sheet generated by a pair of Nd:YAG lasers (200 mJ/pulse, 5 ns pulse duration) and a combination of spherical and cylindrical lenses. A high-energy mirror directs the laser sheet into the wind tunnel such that it is normal to the flow boundary and parallel to the flow direction. The flow is seeded with 1 μm olive oil droplets and time-separated images of the scattered light from the particles are

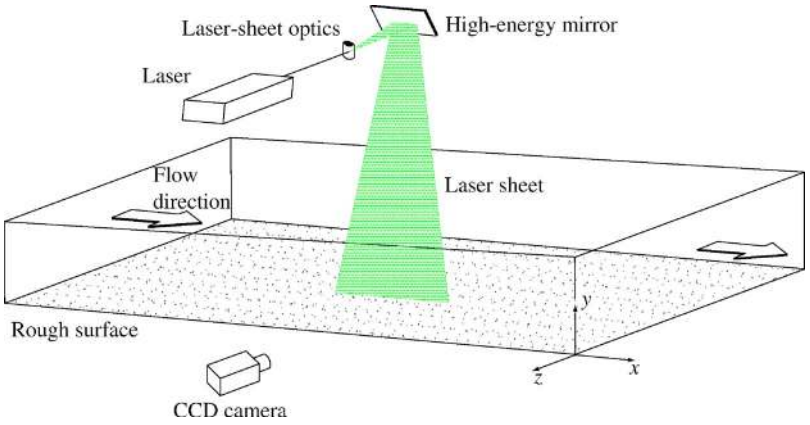

FIG. 2. (Color online) Experimental setup for the PIV measurements in the streamwise–wall-normal (x-y) plane.

captured with a 4k×2.8k, 12-bit frame-straddle CCD camera over a field of view of $1.4\delta\times\delta$ (streamwise by wall-normal). The roughness at the measurement location is painted black to reduce reflections of laser light; however, the remaining unsuppressed reflections render measurements in the region $y<0.08\delta$ and $y<0.05\delta$ unachievable for the RF1 and RF2 cases, respectively. Therefore, smooth-wall data are only presented for $y>0.05\delta$. Table III summarizes the relevant experimental parameters.

The pairs of PIV images are interrogated using two-frame cross-correlation methods. The sizes of the interrogation windows are chosen to maintain a consistent vector grid spacing between the smooth- and rough-wall data when scaled in inner units (i.e., by u_τ and ν) and the second window is offset by the bulk displacement to reduce errors associated with loss of image pairs. As is indicated in Table III, the grid spacing for the smooth- and rough-wall data sets is $\Delta x^+=\Delta y^+=\Delta^+\approx 18$ [where $(\cdot)^+$ denotes normalization in inner units]. The resulting velocity vector fields are then validated using standard deviation and magnitude difference comparisons to remove erroneous velocity vectors. On average, a valid vector yield of 95–97% is achieved, minimizing the need for interpolation of holes. Finally, each velocity field is low-pass filtered with a narrow Gaussian filter to remove noise associated with frequencies larger than the sampling frequency of the interrogation.

The friction velocity, u_τ, for each case (smooth, RF1 and RF2) is determined using the total shear stress method, which assumes a region of constant shear stress equal to the wall shear stress in the overlap and inner region of the boundary layer.[7] In this region of constant shear stress, the friction velocity can be estimated as

$$u_\tau \cong \left(\nu\frac{\partial U}{\partial y}-\overline{u'v'}\right)^{1/2}, \tag{1}$$

where the first and second terms on the right-hand side represent the viscous and turbulent contributions to the total shear stress, respectively. As such, the friction velocity can be deduced from the measured mean velocity and Reynolds shear stress profiles. Values of u_τ estimated in this manner are then used to determine the virtual origin, $y_\circ$, and the roughness function, ΔU^+, for the rough-wall cases by fitting the mean velocity profile to the expected logarithmic profile in the log layer given by

$$U^+=\frac{1}{\kappa}\ln(y^+-y_\circ^+)+A-\Delta U^+, \tag{2}$$

where $\kappa=0.41$ and $A=5.1$ are the log-law constants. Knowledge of ΔU^+ enables one to relate the roughness studied herein to the sand-grain experiments of Nikuradse[11] via an equivalent sand-grain height, k_s^+, that yields the same ΔU^+ as the present rough surfaces through the fully rough asymptote given by

$$\Delta U^+=\frac{1}{\kappa}\ln(k_s^+)+A-8.5. \tag{3}$$

Prasad *et al.*[23] showed that the random error associated with determining particle displacements in PIV is approximately 5% of the particle-image diameter. In the present study, the mean particle-image diameter is approximately two pixels, yielding a random error of 0.1 pixels. Therefore, since the time delay between the PIV images for a given experiment is chosen to yield a bulk displacement of 10–12

TABLE III. Summary of experimental parameters.

Surface	Re_θ	U_e (m/s)	δ (mm)	u_τ (m/s)	δ^+	ΔU^+	k (mm)	k^+	k_s^+	δ/k	δ/k_s	$5k/\delta$	Δ^+
–	–				–	–		–	–	–	–	–	–
Smooth	11940	16.2	104	0.53	3470	–	–	–	–	–	–	–	19
RF1	14780	16.9	112	0.76	5530	8.2	4.2	207	115	27	48	0.188	18
RF2	13690	16.8	110	0.68	4760	4.9	2.1	91	29	52	162	0.094	17

pixels, the random error of the PIV velocity measurements is less than 1% of the full-scale velocity. One must also consider two sources of bias error that can appear in PIV measurements. Bias due to loss of image pairs is minimized in the present study since a larger second interrogation window and a bulk window offset are utilized during interrogation of the PIV images. Bias errors due to the peak-locking effect[24] are also minimized in the present experiment since the particle-image diameters exceed two pixels.[25] We therefore estimate the bias errors in our PIV measurements at 1% of the full-scale velocity (the reader is directed to Westerweel,[25] Christensen and Adrian,[26] and Christensen[24] for a more comprehensive discussion of PIV measurement errors). It should be noted, however, that the uncertainties associated with the velocity measurements are negligible compared to the uncertainty of approximately 6% (Refs. 7 and 27) associated with using the constant shear stress method to estimate u_τ for all three surface conditions. As such, this uncertainty in u_τ represents the dominant uncertainty in all inner-scaled turbulence statistics presented.

III. RESULTS

A. Mean velocity profiles

Inner-scaled mean velocity profiles are presented in Fig. 3(a) for the smooth- and rough-wall cases. The mean velocity profiles are computed by ensemble-averaging the velocity fields for a given case followed by line-averaging in the streamwise direction in a manner similar to other recent PIV studies of rough-wall turbulence.[28,29] As expected, the presence of roughness shifts the logarithmic region of the mean velocity profiles downward by $\Delta U^+=8.2$ and 4.9 and enhances the friction velocity by 43% and 28% relative to the smooth-wall baseline for RF1 and RF2, respectively. Given $\Delta U^+=8.2$ for RF1, in concert with Eq. (3), an equivalent sand-grain height of $k_s^+=115$ is found that places the RF1 case well within the fully rough regime based on accepted historical classifications. The existence of fully rough flow under the present RF1 conditions can be verified by ensuring that the skin friction coefficient, $C_f \equiv 2\tau_w/\rho U_e^2$, has approached a constant value, independent of Re_θ (and hence viscosity since C_f must only depend on the character of the roughness in the fully rough regime[30]). Alternatively, one can evaluate the onset of fully rough flow by verifying that the inner-scaled free-stream velocity, U_e^+, has approached a constant value, independent of Re_θ, since $C_f=2(U_e^+)^{-2}$. Measurements for flow over the same RF1 topography at a slightly lower Reynolds number of $\mathrm{Re}_\theta=9000$ (not shown) give $U_e^+=22.1$ compared to the present case which yields $U_e^+=22.2$. This consistency in U_e^+ supports the notion that the present RF1 case is fully rough. For the RF2 case, $\Delta U^+=4.9$ along with the fully rough asymptote defined in Eq. (3) gives $k_s^+=29$. However, comparing $U_e^+=24.8$ for the present RF2 case with $U_e^+=25.2$ garnered from measurements over the same surface at $\mathrm{Re}_\theta=8330$ (not shown) indicates that the RF2 flow is likely still in transition toward a fully rough state. It should be noted, however, that both RF1 and RF2 satisfy $\delta/k_s > 40$ despite the fact that $\delta/k=28<40$ for RF1. Recall that most studies supporting wall similarity (Table I) exhibit large δ/k_s values and Flack *et al.*[7] proposed $\delta/k_s \gtrsim 40$ as a threshold for wall similarity to exist. In contrast, most studies that do not observe outer-layer similarity suffer from low δ/k_s values despite having large values of δ/k. As such, the present roughness cases allow evaluation of the Flack *et al.*[7] threshold of $\delta/k_s \gtrsim 40$ as well as that of Jimenez[4] ($\delta/k \gtrsim 40$) for the case of more practical surface roughness.

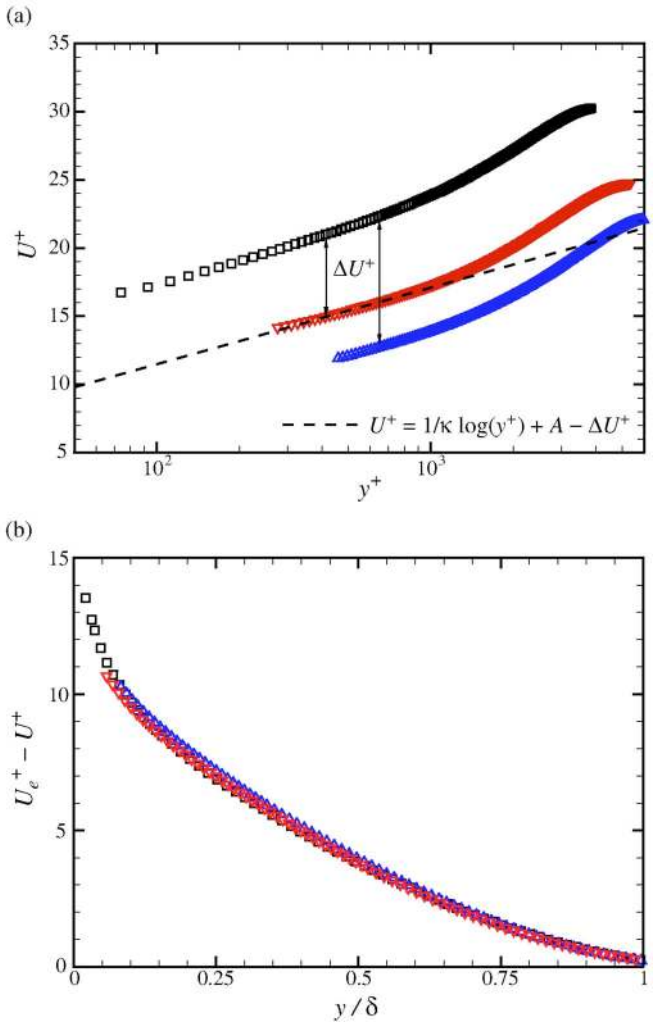

FIG. 3. (Color online) Mean velocity profiles over smooth and rough surfaces. (a) Inner scaling; (b) velocity defect scaling. Not all data points shown for clarity. □, Smooth; △, RF1; ∇, RF2.

Figure 3(b) presents the mean velocity profiles for the smooth and rough cases in velocity defect form ($U_e^+ - U^+$ versus y/δ). Excellent agreement is noted between the two rough-wall velocity defect profiles and the smooth-wall baseline in the overlap and outer layers. This agreement indicates that roughness effects on the mean velocity are confined to the inner layers of the rough-wall flows, supporting the existence of outer-layer similarity. A similar collapse of smooth- and rough-wall mean velocity profiles in defect scaling was also noted recently by Connelly *et al.*[31] for turbulent boundary layers in the presence of sand grain and wire mesh as well as by Allen *et al.*[20] for honed surfaces in turbulent pipe flow.

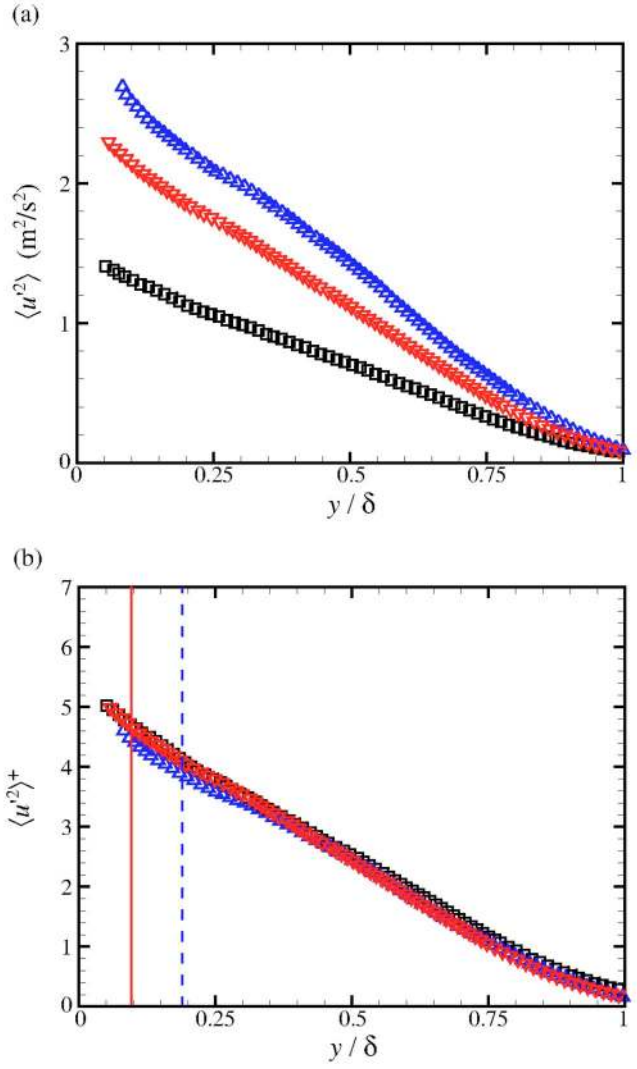

FIG. 4. (Color online) Streamwise Reynolds stress, $\langle u'^2 \rangle$, as a function of wall-normal position over smooth and rough surfaces. (a) Physical units (m^2/s^2); (b) normalized by u_τ^2. Not all data points shown for clarity. Dashed and solid lines in (b) denote the $5k/\delta$ positions for RF1 and RF2, respectively. □, Smooth; △, RF1; ∇, RF2.

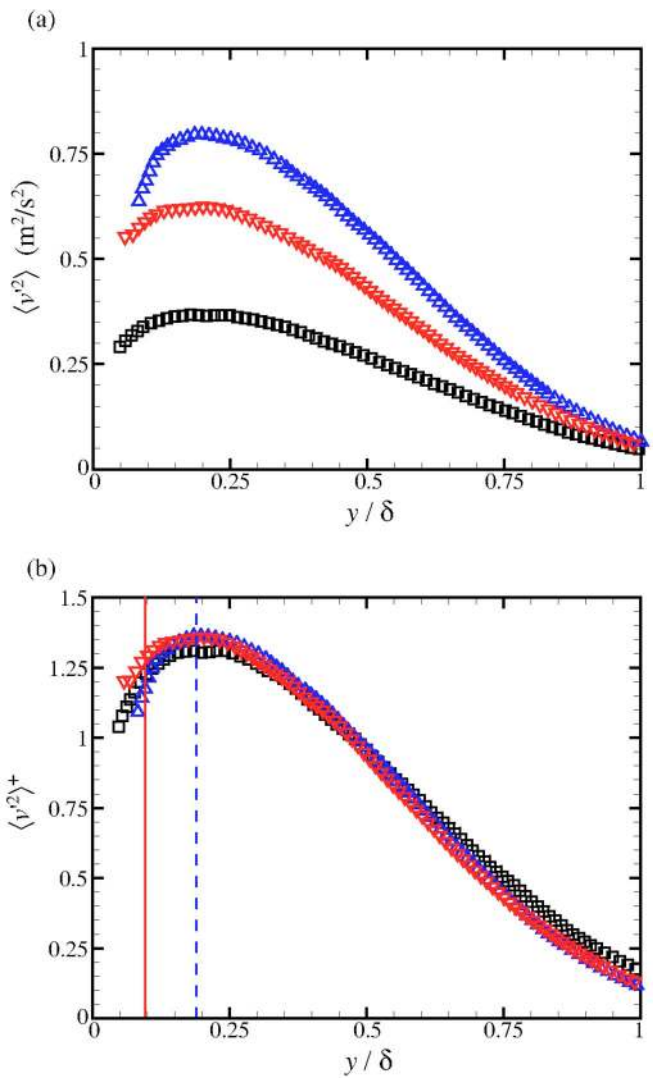

FIG. 5. (Color online) As Fig. 4, but for wall-normal Reynolds normal stress, $\langle v'^2 \rangle$.

B. Reynolds stresses

Profiles of the streamwise Reynolds stress, $\langle u'^2 \rangle$, in physical units as a function wall-normal position are presented in Fig. 4(a) for the smooth, RF1 and RF2 cases. It is clear that roughness significantly augments $\langle u'^2 \rangle$ compared to the smooth-wall baseline. In particular, surface RF1 generates a more substantial enhancement of $\langle u'^2 \rangle$ compared to the RF2 case since its characteristic roughness height is twice that of RF2. A similar enhancement due to roughness is also noted in profiles of the wall-normal Reynolds stress, $\langle v'^2 \rangle$, in physical units [Fig. 5(a)].

When the physical-scale profiles of $\langle u'^2 \rangle$ and $\langle v'^2 \rangle$ are normalized by their respective u_τ^2 values [Figs. 4(b) and 5(b), respectively], excellent collapse is achieved throughout the outer region from the upper extent of the roughness sublayer (demarcated by the vertical lines at the $5k/\delta$ positions for the RF1 and RF2 cases) to the boundary layer edge. This collapse is consistent with the notion of outer-layer similarity wherein the surface conditions set the drag at the boundary (which equivalently sets u_τ) and the turbulence away from the wall adjusts itself to this drag in a universal manner. Similar collapse of rough-wall inner-scaled profiles of $\langle u'^2 \rangle$ and $\langle v'^2 \rangle$ with smooth-wall data was recently reported by Flack *et al.*[7] for flow over sand grain and wire mesh and by Schultz and Flack[27] for flow over close-packed spheres, with all rough-wall conditions satisfying $\delta/k_s > 40$. In addition, Allen *et al.*[20] noted a similar collapse of $\langle u'^2 \rangle^+$ in the outer layer for smooth- and rough-wall (honed surface) turbulent pipe flow for $\delta/k_s \sim 17000$.

Figure 6(a) presents profiles of Reynolds shear stress, $-\langle u'v' \rangle$, in physical units for the smooth and rough cases. As with the Reynolds normal stresses, the RF1 case yields the greatest enhancement of the turbulent shear stress relative to both the smooth-wall baseline and the RF2 case. In particular, RF1 enhances the peak Reynolds shear stress by a factor of 2 relative to the smooth-wall case. When normalized by u_τ^2 [Fig. 6(b)], excellent collapse of the rough-wall profiles on the smooth-wall baseline is achieved outside of the rough-

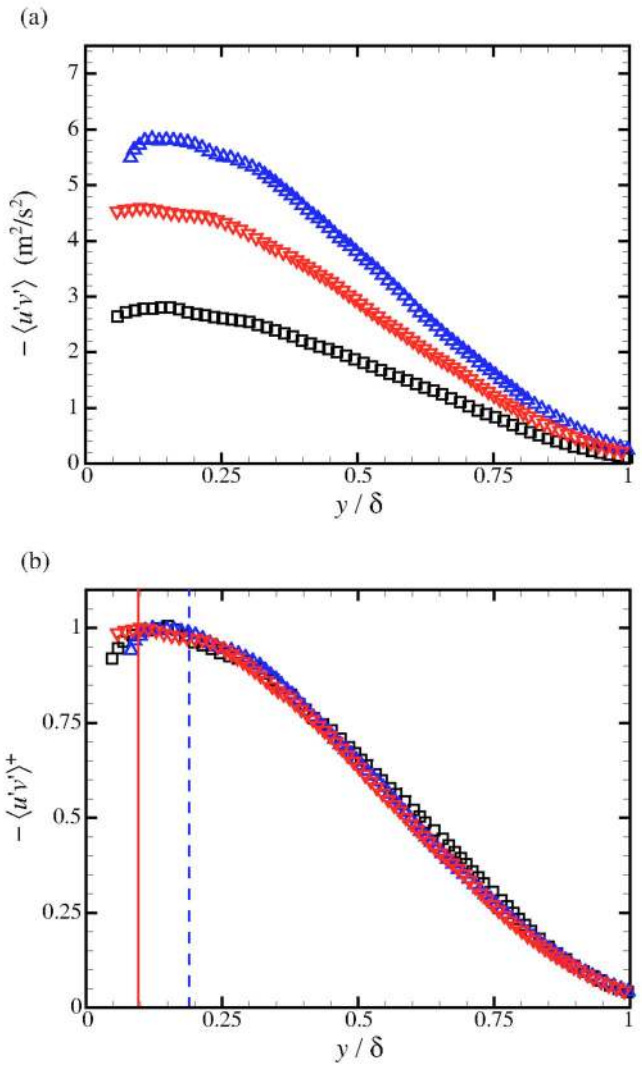

FIG. 6. (Color online) As Fig. 4, but for Reynolds shear stress, $-\langle u'v'\rangle$.

ness sublayer ($y>5k$). This collapse of the mean Reynolds shear stress profiles on u_τ^2 is again consistent with the notion of outer-layer similarity.

Finally, these Reynolds normal and shear stress profiles indicate that the accepted measure for the outer edge of the roughness sublayer from studies of idealized roughness ($\sim 3-5k$) appears to hold well for the roughness studied herein. It should be noted that Flack *et al.*[7] proposed $\sim 5k_s$ as a more consistent measure for the outer extent of the roughness sublayer. However, a lack of data below $5k_s$ in the present experiments does not allow for a detailed evaluation of this possibility for these rough-wall conditions.

C. Quadrant analysis

While the profiles of $\langle u'v'\rangle$ show similarity in the outer region when scaled by u_τ^2, this collapse need not require that the distributions of the instantaneous $u'v'$ events contributing to these mean profiles be identical between the smooth- and rough-wall cases. To explore such issues, we first consider probability density functions (pdf's) of $u'v'$ in physical units as presented in Figs. 7(a) and 7(b) for the smooth and rough cases at $y=0.1\delta$ and 0.25δ, respectively. As expected, the pdf's are notably skewed toward negative values in both the smooth- and rough-wall cases, indicative of the dominant contributions of ejection and sweep events to the overall Reynolds stress profiles shown in Fig. 6. Of particular interest is the noted enhancement of both negative and positive $u'v'$ events in the presence of roughness, particularly in the case of RF1. This enhancement is noted both within the roughness sublayer at $y=0.1\delta$ as well as outside the roughness sublayer at $y=0.25\delta$. Similar enhancement of Reynolds-stress-producing events was noted by Wu and Christensen[32] in fully developed turbulent channel flow encountering a short streamwise fetch of highly irregular roughness replicated from a turbine blade damaged by spallation.

When the instantaneous $u'v'$ events contributing to the pdf's are normalized by u_τ^2, excellent collapse of the pdf's is observed irrespective of surface condition, and this collapse improves as one moves further away from the roughness sublayer [Figs. 7(c) and 7(d) at $y=0.1\delta$ and 0.25δ, respectively]. Therefore, while the mean Reynolds shear stress profiles display clear outer-layer similarity when scaled by u_τ^2 [Fig. 6(b)], the collapse of these $u'v'$ pdf's on u_τ^2 provides strong support for outer-layer similarity in the Reynolds-stress-producing events that contribute to the overall mean profiles.

One can further evaluate the perceived similarity in the Reynolds-stress-producing events by discriminating between the various quadrant events that contribute to the overall mean Reynolds shear stress profile. For example, the negative tails of the pdf's embody contributions from both ejections ($Q2$) and sweeps ($Q4$) while the positive tails contain contributions from both outward ($Q1$) and inward ($Q3$) interactions. To explore possible modifications of these individual quadrant events in the presence of roughness, quadrant analysis, as first proposed by Lu and Willmarth,[33] is applied to the smooth and rough cases. In quadrant analysis, the mean Reynolds shear stress at each wall-normal position is decomposed into contributions from the four quadrants of the u'-v' plane excluding a hyperbolic hole of size H as

$$\langle u'v'\rangle_Q(y;H)=\frac{1}{M}\sum_{j=1}^{M}u(x_j,y)v(x_j,y)I_Q(x_j,y;H), \tag{4}$$

where M is the total number of velocity vectors at each wall-normal position and I_Q is an indicator function defined as

$$I_Q(x_j,y;H)=\begin{cases}1 & \text{when } |u'(x_j,y)v'(x_j,y)|_Q \geq H\sigma_u(y)\sigma_v(y)\\ 0 & \text{otherwise,}\end{cases} \tag{5}$$

where $\sigma_u \equiv \langle u'^2\rangle^{1/2}$ and $\sigma_v \equiv \langle v'^2\rangle^{1/2}$ are root-mean-square streamwise and wall-normal velocities, respectively. The value H represents a threshold on the strength of the Reynolds-stress-producing events considered in the analysis, with $H=0$ allowing all $u'v'$ events to be included in the decomposition and increasing values of H allowing inclusion of only increasingly strong Reynolds-stress-producing events.

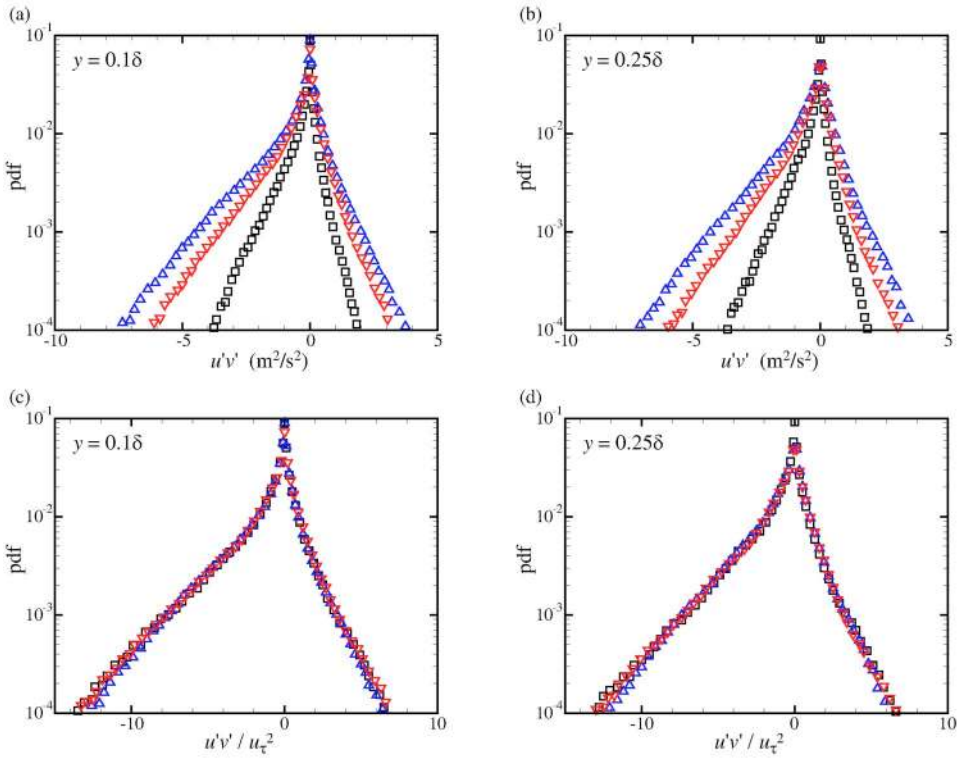

FIG. 7. (Color online) Probability density functions of instantaneous $u'v'$ events (a,b) in physical units (m^2/s^2) and (c,d) normalized by u_τ^2 at $y=0.1\delta$ and 0.25δ, respectively. Not all data points shown for clarity. □, Smooth; △, RF1; ∇, RF2.

The contributions from events of all four quadrants to the Reynolds shear stress, $\langle u'v' \rangle_Q$ ($Q=1-4$), with $H=0$ are presented in Figs. 8(a) and 8(b) for the smooth and rough cases. The smooth-wall results are consistent with past studies of smooth-wall turbulence: $Q2$ (ejection) and $Q4$ (sweep) events contribute heavily to the mean Reynolds shear stress compared to $Q1$ (outward interaction) and $Q3$ (inward interaction) events. When the rough-wall contributions are compared to the smooth-wall baseline, excellent collapse is observed outside the roughness sublayer ($y>5k$) for all four quadrant events when appropriately scaled by u_τ^2, consistent with the outer-layer similarity observed in the mean Reynolds shear stress [Fig. 6(b)]. This outer-layer collapse is also consistent with the quadrant-analysis results of Flack *et al.*[7]

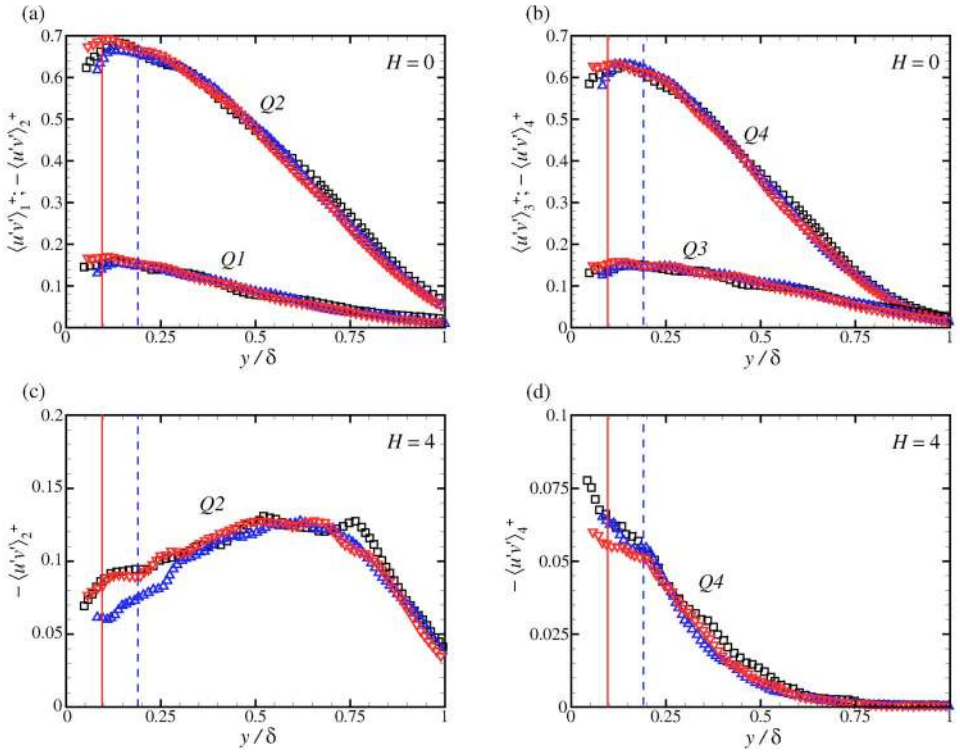

FIG. 8. (Color online) Quadrant contributions to the mean Reynolds shear stress, $\langle u'v' \rangle_Q^+$, as a function of wall-normal position for (a,b) $H=0$ and (c,d) $H=4$. Lines as in Fig. 4 and not all data points shown for clarity. □, Smooth; △, RF1; ∇, RF2.

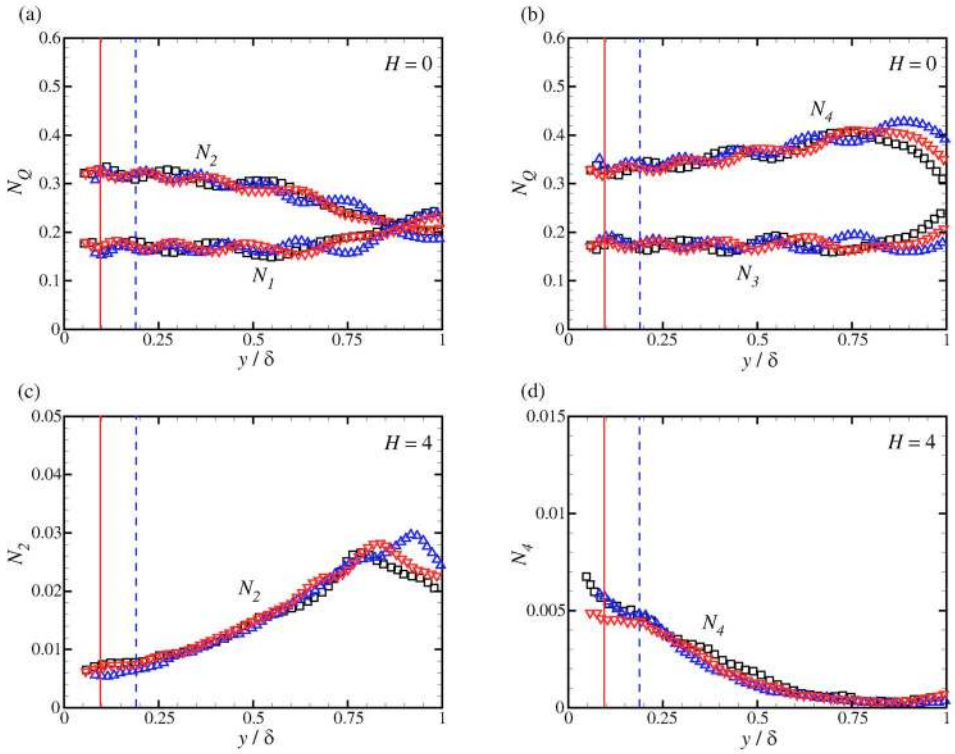

FIG. 9. (Color online) Space fractions, N_Q, as a function of wall-normal position for (a,b) $H=0$ and (c,d) $H=4$. Lines as in Fig. 4 and not all data points shown for clarity. □, Smooth; △, RF1; ∇, RF2.

for flow over sand-grain and wire-mesh topographies. In contrast, Krogstad *et al.*[12] observed that the contributions from $Q2$ and $Q4$ events were enhanced by wire-mesh roughness across most of the outer layer compared to smooth-wall turbulence. It should be noted that the roughness considered in Krogstad *et al.*[12] was quite strong as evidenced by a relatively weak scale separation of $\delta/k_s=15$.

Figures 8(c) and 8(d) present the $Q2$ and $Q4$ contributions to the mean Reynolds shear stress for $H=4$, meaning only the most intense $u'v'$ events are included (the contributions from $Q1$ and $Q3$ events are nearly zero for $H=4$ and are therefore not presented). As with the $H=0$ case, reasonable agreement between the smooth and rough cases is observed outside the roughness sublayer ($y>5k$). These profiles have slightly wider scatter than the $H=0$ profiles simply because there are many fewer $u'v'$ events that satisfy the intense threshold of $H=4$. This scatter is most apparent in the $Q2$ contributions to the mean Reynolds shear stress for $H=4$ [Fig. 8(c)], although the variations relative to the smooth-wall baseline are within the estimated uncertainty for this statistic (~10–15% due the relatively small sample size). Therefore, outer-layer similarity appears to hold for even the most intense Reynolds-stress-producing events. Similar collapse outside the roughness sublayer (with comparable scatter) was also observed by Flack *et al.*[7] for $H=4$ quadrant contributions in the presence of sand grain and wire mesh.

The collapse observed in the mean Reynolds shear stress profile, the pdf's of the instantaneous Reynolds-stress-producing events, and the quadrant contributions to the mean Reynolds shear stress provide significant evidence that the Reynolds-stress-producing events over smooth and rough walls are similar. One question still remains, however, related to the fraction of space in the flow occupied by these Reynolds-stress-producing events for smooth- and rough-wall turbulence. One can define a space fraction, $N_Q(y;H)$, for a given H as

$$N_Q(y;H)=\frac{\sum I_Q(y;H)}{M}, \tag{6}$$

where I_Q is given by Eq. (5) and M is the total number of sample points at a given wall-normal location. Figures 9(a) and 9(b) present the space fractions for $Q1-Q4$ events for $H=0$. The smooth- and rough-wall space fractions display strong consistency in the outer layer, indicating that a similar fraction of space in the flow is occupied by the various quadrant events despite markedly different surface conditions. Similar collapse is noted in the space fractions for the most intense Reynolds-stress-producing events ($H=4$) as presented in Figs. 9(c) and 9(d) for $Q2$ and $Q4$ events, respectively (the space fractions for $Q1$ and $Q3$ events are nearly zero for $H=4$ and are therefore not presented).

Finally, the ratio of the contributions from $Q2$ events to contributions from $Q4$ events,

$$\alpha(y;H)=\frac{\langle u'v'\rangle_2(y;H)}{\langle u'v'\rangle_4(y;H)}, \tag{7}$$

quantifies the relative importance of these events at a given wall-normal position for a given hole size, H. Figures 10(a) and 10(b) present α for the smooth and rough cases at $H=0$ and 4, respectively. For $H=0$, α collapses across the outer layer except very near $y=\delta$, where extremely small differences in the Reynolds shear stress contributions are magnified. Values of α from the wire-mesh studies of Krogstad *et al.*[12] are included for comparison, and consistency is noted with the present results. For $H=4$, the profiles

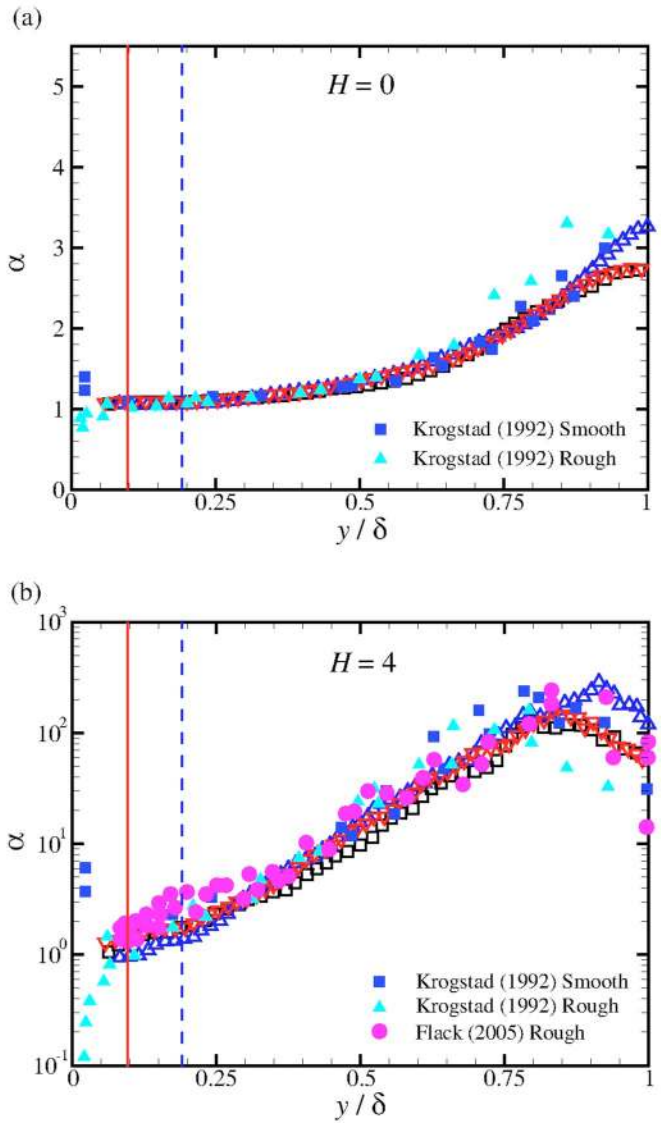

FIG. 10. (Color online) Ratio of Reynolds-shear-stress contributions from $Q2$ and $Q4$ events, α, as a function of wall-normal position for (a) $H=0$ and (b) $H=4$. Lines as in Fig. 4 and not all data points shown for clarity. □, Smooth; △, RF1; ∇, RF2.

of α show good collapse in classic semilog form. The α results of Flack *et al.*[7] and Krogstad *et al.*[12] are also included for comparison and agree well with the present results except very close to the wall. It should be noted that while Krogstad *et al.*[12] observed noted modifications in the individual Reynolds-stress contributions of ejection and sweep events, these modifications still yielded α profiles that were consistent between smooth- and rough-wall flows except very close to the wall, where substantial differences were noted.

D. Two-point velocity autocorrelation coefficients

The single-point statistics presented above show strong similarity between the smooth- and rough-wall cases in the outer layer, consistent with many past studies of idealized roughness topographies (see Table I). However, a question still remains as to whether the *spatial structure* of these flows is similar in the outer layer as well. In particular, understanding modifications of the spatial character of the flow by roughness is important as many turbulence models [large-eddy simulation (LES) subgrid-scale models, for example] and control strategies rely heavily on details of the flow's spatial structure. Past studies of wall turbulence indicate that the two-point autocorrelation coefficients of streamwise and wall-normal velocity, ρ_{uu} and ρ_{vv}, given by

$$\rho_{uu}(r_x,y;y_{\mathrm{ref}}) = \frac{\langle u'(x,y_{\mathrm{ref}})u'(x+r_x,y)\rangle}{\sigma_u(y_{\mathrm{ref}})\sigma_u(y)} \tag{8}$$

and

$$\rho_{vv}(r_x,y;y_{\mathrm{ref}}) = \frac{\langle v'(x,y_{\mathrm{ref}})v'(x+r_x,y)\rangle}{\sigma_v(y_{\mathrm{ref}})\sigma_v(y)}, \tag{9}$$

mimic the average spatial characteristics of the underlying flow structure. In Eqs. (8) and (9), r_x is the spatial separation in the streamwise direction, y_{ref} is the fixed wall-normal position at which the correlation maps are calculated, and σ_u and σ_v are the root-mean-square streamwise and wall-normal velocities, respectively.

Many recent experimental and computational studies support the existence of hairpin-like vortices in smooth-wall turbulence that streamwise align to form larger-scale entities termed hairpin vortex packets (see Refs. 34 and 35, for example). When sliced in the streamwise–wall-normal plane, these packets are characterized by an inclined interface formed by a series of streamwise-aligned spanwise vortex cores that are the imprint of the heads of the individual hairpin-like structures. Each hairpin structure generates an intense ejection of low-speed fluid away from the wall, which contributes significantly to the generation of Reynolds shear stress. In addition, a large-scale region of streamwise momentum deficit is observed below the inclined interface due to the collective induction of the vortices. Christensen *et al.*[36] showed that the spatial characteristics of ρ_{uu} in the (r_x,y) plane mimic those of large-scale vortex packets both in streamwise extent and inclination angle. In addition, this effort also revealed a clear consistency between the spatial extent of ρ_{vv} and the individual spanwise vortices. Therefore, modifications of ρ_{uu} and/or ρ_{vv} by roughness would be indicative of possible modifications of the underlying spatial structure of the flow.

While a vast majority of the rough-wall literature has focused on the impact of roughness on the single-point statistics, a few of these efforts have also assessed the impact of idealized roughness on the average spatial character of the flow, typically via two-point autocorrelations of velocity. Krogstad and Antonia[37] observed a significant reduction in the streamwise extents of ρ_{uu} and ρ_{vv} both within the roughness sublayer and in the outer layer (as inferred from time series of velocity acquired by cross-wire probes) in the presence of woven mesh with $k_s^+=331$ and $\delta/k_s=15$. This effort also reported a drastic increase in the inclination angle of ρ_{uu} in the (r_x,y) plane under rough-wall conditions. In contrast, the recent PIV measurements of fully rough flow over a wavy surface by Nakagawa and Hanratty[28] indicate a strong similarity in the streamwise extent and inclination angle of ρ_{uu} as well as the spatial extent of ρ_{vv} in the outer layer when

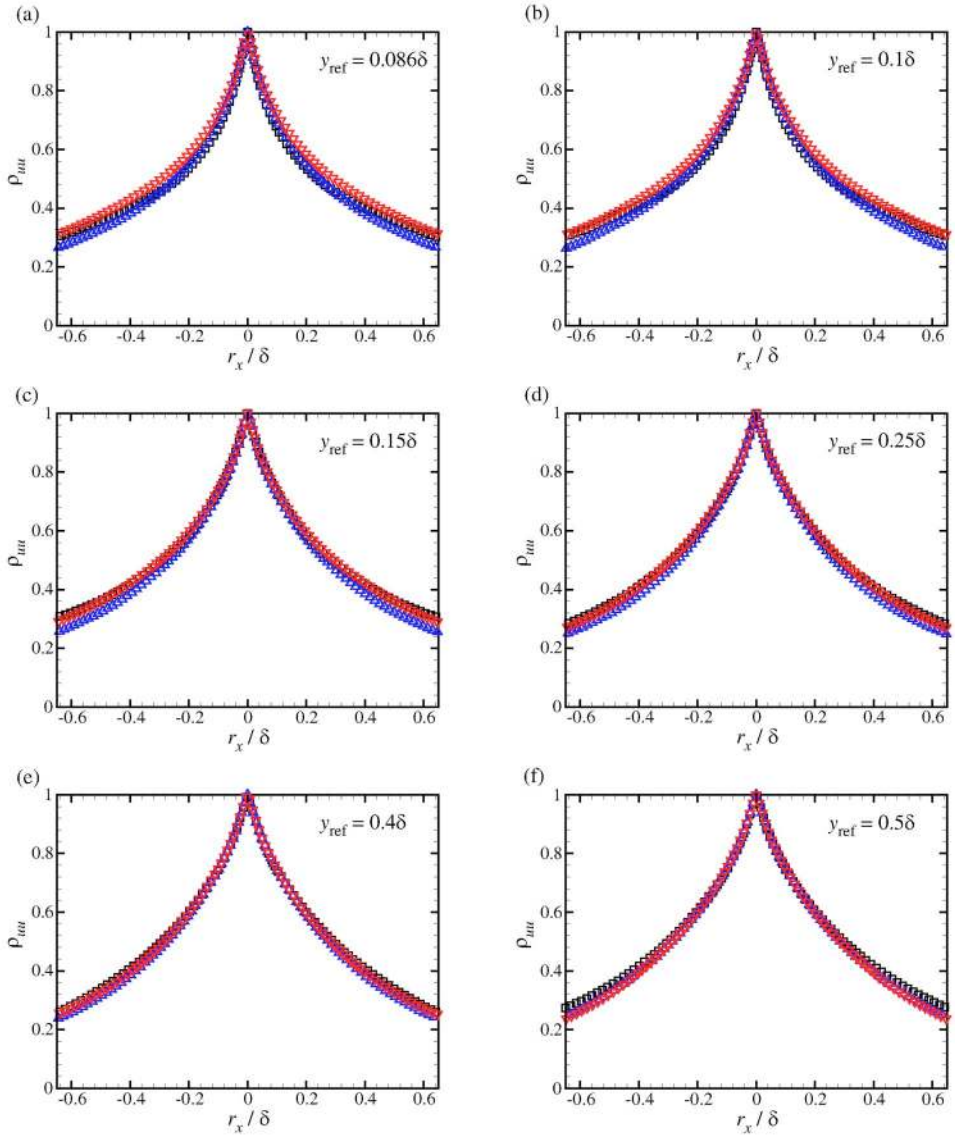

FIG. 11. (Color online) Streamwise velocity autocorrelation coefficients, ρ_{uu}, at (a) $y=0.086\delta$, (b) $y=0.1\delta$, (c) $y=0.15\delta$, (d) $y=0.25\delta$, (e) $y=0.4\delta$, and (f) $y=0.5\delta$. Not all data points shown for clarity. □, Smooth; △, RF1; ∇, RF2.

compared to similar features in smooth-wall turbulence. Nakagawa and Hanratty[28] hypothesize that the stark differences between their observations and those of Krogstad and Antonia[37] may be partially attributable to the assumption of a constant convection velocity by Krogstad and Antonia[37] in the application of Taylor's hypothesis to infer spatial variations of the autocorrelations from time-series data. Finally, Allen *et al.*[20] reported strong outer-layer similarity in streamwise velocity spectra for smooth- and rough-wall (honed surface) turbulent pipe flow for $\delta/k_s \sim 17000$, indicating a negligible impact of roughness on the outer-layer structure under these conditions.

The characteristic streamwise extents of ρ_{uu} and ρ_{vv} can be assessed by plotting their one-dimensional profiles for fixed wall-normal position (i.e., $y=y_{ref}$). Figures 11(a)–11(f) present one-dimensional profiles of ρ_{uu} at $y/\delta=0.086$, 0.1, 0.15, 0.25, 0.4, and 0.5, respectively, as a function of r_x/δ for the smooth and rough cases. The wall-normal location $y=0.086\delta$ is chosen for comparison because it is the closest position to the wall for which data are available for all three cases. Also note that the first three wall-normal locations are within the roughness sublayer defined by $y<5k$ for the RF1 case while the first two wall-normal positions are inside the roughness sublayer for the RF2 case. Near the wall, subtle differences exist between the smooth-wall baseline and the rough-wall cases. In particular, ρ_{uu} is enhanced slightly at moderate r_x for the RF2 case but diminished slightly for the RF1 case relative to the smooth-wall baseline. Therefore, the characteristic streamwise length scale of ρ_{uu}, representative of the streamwise extent of outer-layer vortex organization, is enhanced slightly by RF2 but diminished by RF1 relative to the smooth-wall baseline. Recall that the most obvious distinction between RF1 and RF2 is the factor of 2 difference in the characteristic roughness height, k, which places RF1 in the fully rough regime and RF2 in the transitionally rough regime. However, this factor of 2 scaling of RF1 relative to RF2 is not only reflected in k but also in the characteristic *spacing* of the dominant topographical features of the roughness in the streamwise and spanwise directions. As such, the opposing impacts of RF1 and RF2 on ρ_{uu} in the roughness sublayer may be attributable to one or both of these differences. From a structural viewpoint, these slight differences in

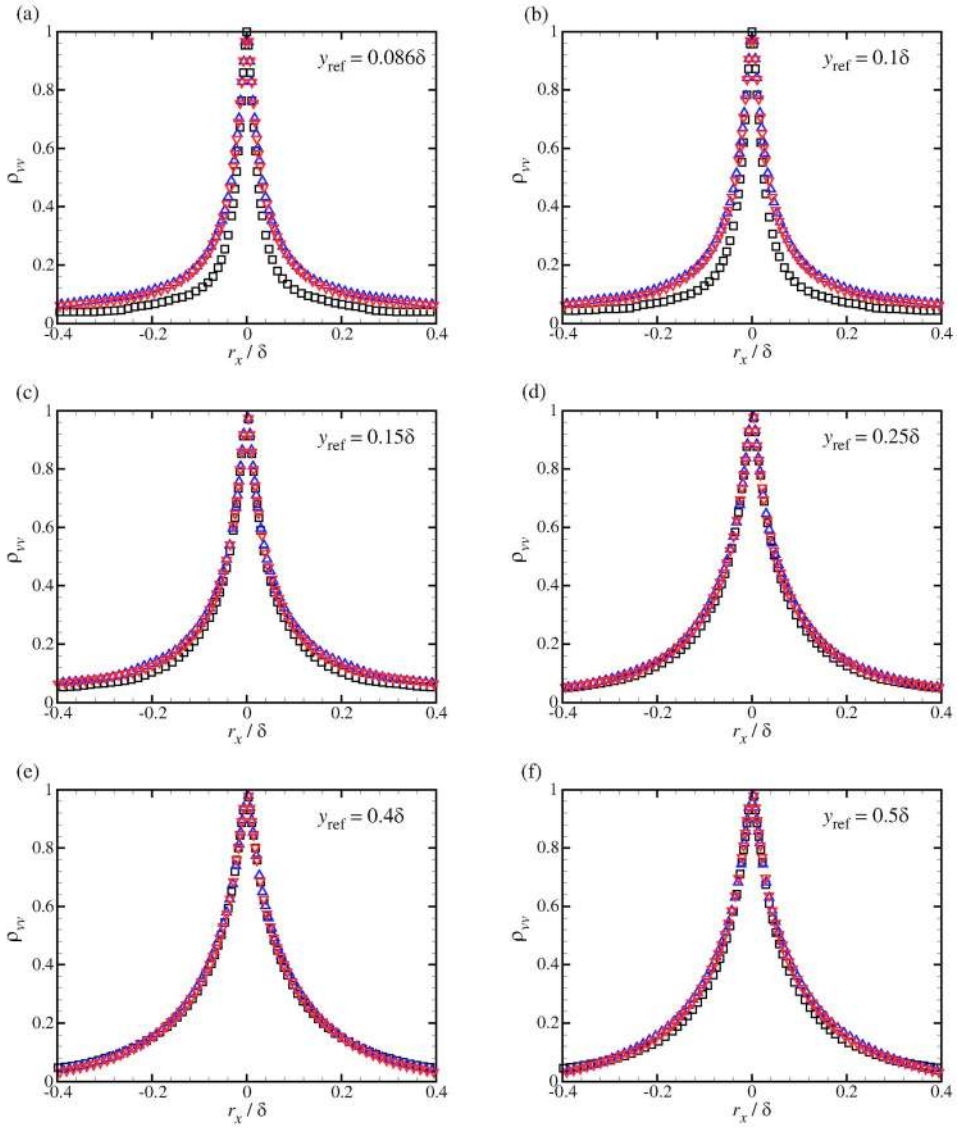

FIG. 12. (Color online) As Fig. 11 but for wall-normal velocity autocorrelation coefficients, ρ_{vv}.

ρ_{uu} within the roughness sublayer may be tied to a roughness-induced modification of the hairpin vortex regeneration mechanism thought to drive the formation and sustainment of coherent vortex packets.[35,38]

Nevertheless, these roughness effects diminish significantly as the outer layer is approached, with RF2 displaying similarity with the smooth case for $y > 0.1\delta$ and RF1 showing similarity for $y > 0.25\delta$. This outer-layer similarity in ρ_{uu} is quite consistent with the observations of Nakagawa and Hanratty[28] for fully rough flow over a wavy surface but certainly inconsistent with the drastic reduction in the streamwise extent of ρ_{uu} observed by Krogstad and Antonia[37] for fully rough flow over wire mesh. While Nakagawa and Hanratty[28] attributed these differences to the use of time-series data to infer the character of spatial correlations, these differences may also be due to the weak scale separation ($\delta/k_s = 15$) present in the Krogstad and Antonia[37] experiments.

Figure 12 presents ρ_{vv} at $y/\delta = 0.086$, 0.1, 0.15, 0.25, 0.4, and 0.5, respectively, for the smooth and rough cases. While roughness has a relatively subtle influence on ρ_{uu}, it has a much more dramatic impact on ρ_{vv}. In particular, roughness increases the characteristic width of ρ_{vv} close to the wall for both roughness cases. In the context of the underlying spatial structure, roughness appears to increase the spatial extent over which the spanwise vortex cores (believed to be the imprint of hairpin heads) exert their influence. This roughness effect diminishes as one moves away from the wall, with excellent collapse occurring for $y \geq 0.25\delta$. It should be noted that while ρ_{uu} collapsed outside the roughness sublayer for the RF2 case ($y > 0.1\delta$), collapse between the RF2 and smooth cases for ρ_{vv} is not noted until $y = 0.25\delta$. Finally, while RF1 and RF2 yield opposing effects on ρ_{uu}, they produce a nearly identical enhancement of ρ_{vv} for moderate r_x despite a factor of 2 difference in their characteristic roughness scales. This noted enhancement of the streamwise extent of ρ_{vv} within the roughness sublayer is counter to the reduction in the spatial extent of ρ_{vv} reported by Krogstad and Antonia[37] for flow over wire mesh (both within and outside the roughness sublayer) while the outer-layer similarity

in ρ_{vv} reported herein is consistent with the outer-layer similarity reported by Nakagawa and Hanratty[28] for flow over a wavy surface.

IV. SUMMARY AND CONCLUSIONS

High-resolution PIV measurements are performed in the streamwise–wall-normal plane of a zero-pressure-gradient turbulent boundary layer over both smooth and rough walls at $\mathrm{Re}_\theta \approx 13000$. Of particular interest is the fact that the roughness studied herein is quite distinct from the idealized topographies normally studied in the laboratory (sand grain, wire mesh, etc.) in that it is highly irregular and contains a broad range of topographical scales. Inner-scaled mean velocity profiles over the rough surfaces display the expected downward shift of the log region by the roughness function ΔU^+. In addition, the mean velocity profiles are found to collapse in velocity defect scaling irrespective of surface condition. This collapse supports the existence of outer-layer similarity in the presence of the roughness studied herein.

The Reynolds normal and shear stresses are found to be significantly enhanced by the roughness in an absolute sense, particularly for the RF1 case. However, excellent collapse of these stress profiles is noted outside the roughness sublayer when scaled by u_τ^2, supporting the notion of wall similarity. Similar collapse is noted when quadrant analysis is used to assess the contributions from various Reynolds-stress-producing events to the overall mean Reynolds shear stress. These observations of outer-layer similarity in the Reynolds stresses represent the first of their kind for a highly irregular surface topography at moderate δ/k_s that is representative of what one might encounter in a broad range of technologically relevant flows.

In addition, two-point autocorrelations of streamwise and wall-normal velocity fluctuations indicate a modification of the underlying spatial structure of the flow within the roughness sublayer, particularly a noted enhancement in the streamwise extent of ρ_{vv} for both rough-wall cases. In contrast, the effects of the two roughness cases on ρ_{uu} in the roughness sublayer are counter to one another, with RF2 yielding a slight enhancement in the streamwise extent of ρ_{uu} relative to the smooth-wall baseline as compared to a slight reduction produced by RF1. Despite these noted differences in the roughness sublayer, similarity is noted in both ρ_{uu} and ρ_{vv} when the smooth- and rough-wall cases are compared in the outer layer, consistent with the observations of Nakagawa and Hanratty[28] for flow over a wavy surface as well as the similarity noted in streamwise velocity spectra for smooth- and rough-wall turbulent pipe flow by Allen *et al.*[20] Therefore, while the underlying structure of the turbulence appears modified slightly in the roughness sublayer, particularly an increase in the spatial extent over which individual hairpin-like vortices exert their influence (as inferred from ρ_{vv}), the length scales of the outer-layer structure appear minimally affected in the presence of the roughness topography presented herein.

Further, the present results suggest that the classical measure of ~ 3–$5k$ for the outer extent of the roughness sublayer as determined from idealized roughness studies holds well for the more practical roughness topography studied herein. Unfortunately, while it was recently proposed by Flack *et al.*[7] that $\sim 5k_s$ may be a more consistent measure of the roughness sublayer's outer boundary, a lack of data below $5k_s$ in the present effort does not allow a proper evaluation of this proposition. Finally, it should be noted that wall similarity is noted in both the RF1 and RF2 cases, despite the fact that $\delta/k = 28 < 40$ for RF1. In terms of δ/k_s, both RF1 and RF2 satisfy the threshold of $\delta/k_s > 40$ proposed by Flack *et al.*[7] for the existence of wall similarity. Therefore, the present results lend further support to the importance of δ/k_s, rather than δ/k, in assessing whether wall similarity should be expected in a rough-wall flow.

ACKNOWLEDGMENTS

This work is supported by the Air Force Office of Scientific Research under Grant Nos. FA9550-05-1-0043 and FA9550-05-1-0246 (Dr. John Schmisseur, Program Manager) and the University of Illinois. The roughness sample under consideration was graciously loaned to us by Professor J. Bons of Brigham Young University.

[1] J. P. Bons, "St and C_f augmentation for real turbine roughness with elevated freestream turbulence," J. Turbomach. **124**, 632 (2002).
[2] R. I. Karlsson, "Studies of skin friction in turbulent boundary layers on smooth and rough walls," Ph.D. thesis, Chalmers University of Technology, Göteborg, Sweden (1980).
[3] M. R. Raupach, R. A. Antonia, and S. Rajagopalan, "Rough-wall turbulent boundary layers," Appl. Mech. Rev. **44**, 1 (1991).
[4] J. Jimenez, "Turbulent flow over rough walls," Annu. Rev. Fluid Mech. **36**, 173 (2004).
[5] A. A. Townsend, *The Structure of Turbulent Shear Flow*, 2nd ed. (Cambridge University Press, Cambridge, UK, 1976).
[6] M. R. Raupach, "Conditional statistics of Reynolds stress in rough-wall and smooth-wall turbulent boundary layers," J. Fluid Mech. **108**, 363 (1981).
[7] K. A. Flack, M. P. Schultz, and T. A. Shapiro, "Experimental support for Townsend's Reynolds number similarity hypothesis on rough walls," Phys. Fluids **17**, 035102 (2005).
[8] A. E. Perry and J. D. Li, "Experimental support for the attached-eddy hypothesis in zero-pressure-gradient turbulent boundary layers," J. Fluid Mech. **218**, 405 (1990).
[9] P. M. Ligrani and R. J. Moffat, "Structure of transitionally rough and fully rough turbulent boundary layers," J. Fluid Mech. **162**, 69 (1986).
[10] P. R. Bandyopadhyay and R. D. Watson, "Structure of rough-wall turbulent boundary layers," Phys. Fluids **31**, 1877 (1988).
[11] J. Nikuradse, "Laws of flow in rough pipes," NACA Technical Memorandum No. 1292 (1933).
[12] P. A. Krogstad, R. A. Antonia, and L. W. B. Browne, "Comparison between rough and smooth-wall turbulent boundary layers," J. Fluid Mech. **245**, 599 (1992).
[13] H. S. Shafi and R. A. Antonia, "Small-scale characteristics of a turbulent boundary layer over a rough wall," J. Fluid Mech. **342**, 263 (1997).
[14] P. A. Krogstad and R. A. Antonia, "Surface roughness effects in turbulent boundary layers," Exp. Fluids **27**, 450 (1999).
[15] L. Keirsbulck, L. Labraga, A. Mazouz, and C. Tournier, "Surface roughness effects on turbulent boundary layer structures," J. Fluids Eng. **124**, 127 (2002).
[16] J. P. Bons, R. P. Taylor, S. T. McClain, and R. B. Rivir, "The many faces of turbine surface roughness," J. Turbomach. **123**, 739 (2001).
[17] C. F. Colebrook, "Turbulent flow in pipes with particular reference to the transition region between the smooth- and rough-wall laws," J. Inst. Civil Eng. **11**, 133 (1939).
[18] M. Acharya, J. Bornstein, and M. P. Escudier, "Turbulent boundary layers on rough surfaces," Exp. Fluids **4**, 33 (1986).
[19] C. S. Subramanian, P. I. King, M. F. Reeder, S. Ou, and R. B. Rivir, "Effects of strong irregular roughness on the turbulent boundary layer," Flow, Turbul. Combust. **72**, 349 (2004).

[20] J. J. Allen, M. A. Shockling, G. J. Kunkel, and A. J. Smits, "Turbulent flow in smooth and rough pipes," Philos. Trans. R. Soc. London, Ser. A **365**, 699 (2007).
[21] C. D. Meinhart, "Investigation of turbulent boundary-layer structure using particle-image velocimetry," Ph.D. thesis, University of Illinois at Urbana-Champaign (1994).
[22] R. A. Antonia and R. E. Luxton, "The response of a turbulent boundary layer to a step change in surface roughness. Part 1: Smooth to rough," J. Fluid Mech. **48**, 721 (1971).
[23] A. K. Prasad, R. J. Adrian, C. C. Landreth, and P. W. Offutt, "Effect of resolution on the speed and accuracy of particle image velocimetry interrogation," Exp. Fluids **13**, 105 (1992).
[24] K. T. Christensen, "The influence of peak-locking errors on turbulence statistics computed from PIV ensembles," Exp. Fluids **36**, 484 (2004).
[25] J. Westerweel, "Fundamentals of digital particle image velocimetry," Meas. Sci. Technol. **8**, 1379 (1997).
[26] K. T. Christensen and R. J. Adrian, "Measurement of instantaneous Eulerian acceleration fields by particle-image accelerometry: Method and accuracy," Exp. Fluids **33**, 759 (2002).
[27] M. P. Schultz and K. A. Flack, "Outer layer similarity in fully rough turbulent boundary layers," Exp. Fluids **38**, 328 (2005).
[28] S. Nakagawa and T. J. Hanratty, "Particle image velocimetry measurements of flow over a wavy wall," Phys. Fluids **13**, 3504 (2001).
[29] F. Bigillon, Y. Niño, and M. H. Garcia, "Measurements of turbulence characteristics in an open-channel flow over a transitionally-rough bed using particle-image velocimetry," Exp. Fluids **41**, 857 (2006).
[30] H. Schlichting, *Boundary-Layer Theory* (McGraw-Hill, New York, 1979).
[31] J. S. Connelly, M. P. Schultz, and K. A. Flack, "Velocity-defect scaling for turbulent boundary layers with a range of relative roughness," Exp. Fluids **40**, 188 (2006).
[32] Y. Wu and K. T. Christensen, "Reynolds-stress enhancement associated with a short fetch of roughness in wall turbulence," AIAA J. **44**, 3098 (2006).
[33] S. S. Lu and W. W. Willmarth, "Measurements of the structure of the Reynolds stress in a turbulent boundary layer," J. Fluid Mech. **60**, 481 (1973).
[34] R. J. Adrian, C. D. Meinhart, and C. D. Tomkins, "Vortex organization in the outer region of the turbulent boundary layer," J. Fluid Mech. **422**, 1 (2000).
[35] J. Zhou, C. D. Meinhart, S. Balachandar, and R. Adrian, "Formation of coherent hairpin packets in wall turbulence," in *Self-Sustaining Mechanisms of Wall Turbulence*, edited by R. L. Panton (Computational Mechanics, Southampton, UK, 1997), pp. 109–134.
[36] K. T. Christensen, Y. Wu, R. J. Adrian, and W. Lai, "Statistical imprints of structure in wall turbulence," AIAA Pap. 2004-1116 (2004).
[37] P. A. Krogstad and R. A. Antonia, "Structure of turbulent boundary layers on smooth and rough walls," J. Fluid Mech. **277**, 1 (1994).
[38] J. Zhou, R. J. Adrian, and S. Balachandar, "Autogeneration of near-wall vortical structures in channel flow," Phys. Fluids **8**, 288 (1996).
[39] M. P. Schultz and K. A. Flack, "Turbulent boundary layers over surfaces smoothed by sanding," J. Fluids Eng. **125**, 863 (2003).
[40] A. J. Grass, "Structural features of turbulent flow over smooth and rough boundaries," J. Fluid Mech. **50**, 233 (1971).
[41] P. A. Krogstad, H. I. Andersson, O. M. Bakken, and A. Ashrafian, "An experimental and numerical study of channel flow with rough walls," J. Fluid Mech. **530**, 327 (2005).
[42] O. M. Bakken, P. A. Krogstad, A. Ashrafian, and H. I.Andersson, "Reynolds number effects in the outer layer of the turbulent flow in a channel with rough walls," Phys. Fluids **17**, 065101 (2005).
[43] M. F. Tachie, D. J. Bergstrom, and R. Balachandar, "Roughness effects in low-Re_θ open-channel turbulent boundary layers," Exp. Fluids **35**, 338 (2003).
[44] M. F. Tachie, D. J. Bergstrom, and R. Balachandar, "Rough wall turbulent boundary layers in shallow open channel flow," J. Fluids Eng. **122**, 533 (2000).
[45] K. Bhaganagar, J. Kim, and G. Coleman, "Effect of roughness on wall-bounded turbulence," Flow, Turbul. Combust. **72**, 463 (2004).